UPDATED AREA FUNCTION ANALYSIS FOR NANO INDENTATION OF MICRO FIBERS

By

PRASHANTH TURLA

A thesis submitted to the

Graduate School – New Brunswick

Rutgers, the State University of New Jersey

In partial fulfillment of the requirements

For the degree of

Master of Science

Graduate Program in Mechanical and Aerospace Engineering

Written under direction of

Assimina A. Pelegri

And approved by

New Brunswick, New Jersey

October 2017

ABSTRACT OF THE THESIS

UPDATED AREA FUNCTION ANALYSIS FOR NANO INDENTATION OF MICRO FIBERS

By

PRASHANTH TURLA

Thesis Director:

Professor Assimina A. Pelegri

Kevlar has a remarkable combination of high strength, high modulus, toughness and thermal stability compared to many other organic fibers. These impressive properties are due to their molecular structure, developed during their production process which is based on liquid crystal technology, as the rigid molecular chains form a mesophase in solution. Modeling of the high-performance ballistic fabric has gradually shifted from the continuum and yarn length scales to the sub-yarn length scale which enabled establishment of the relationships between the fabric penetration resistance and various fiber-level phenomena such as fiber-fiber friction, fiber twist, and transverse properties of the fibers.

An instrumented indentation method was established in this thesis work to accurately measure the local elastic-plastic material properties of a single fiber. As indentation theory assumes that the indent is being placed on a semi-infinite flat surface, general area function cannot predict accurate projected area on a circular specimen. The indentations on cylindrical surface require modified equations to determine the area function and subsequently, the hardness and reduced modulus.

The Oliver-Pharr instrumented indentation data analysis method is followed for the calculation of area function of the indenter geometry through the simulation of the known properties of the material. This new area function calculation method is compared with the geometry correction method by Quinn McAllister and John W. Gillespie, Jr to calculate the elastic modulus of the fiber in transverse direction. In addition, Compliance contributions are attributed to the lack of constraint due to the finite geometry of a curved fiber surface. This compliance contribution is accounted by using a proposed area correction to capture the geometry of the curved fiber-probe contact. Implementation of these corrections to experimental indentation curves results in accurate measurements of the fiber elastic modulus.

Acknowledgements

Firstly, I’d like to express my profound gratitude to my advisor and mentor Prof. Assimina A. Pelegri for the relentless support throughout my project, for her motivation, guidance, patience and giving me the freedom to explore on my own.

I would like to thank my committee members Alberto Cuitino and Jonathan Singer for taking time to review this project and serving as a member of the committee.

I would like to thank Daniel Sullivan for helping me with concepts and insights; Max Tenorio for aiding me with the indentation data and experiments; I profusely thank the Mechanical Engineering department of Rutgers University for providing me a platform to study and perform sophisticated research.

I would like to thank all of my teachers who helped me to enhance my knowledge and technical skills.

Finally, I’d like to thank my parents and sister to whom this thesis is dedicated, for being the ultimate source of unconditional love, concern, support and motivation.

TABLE OF CONTENTS

LIST OF FIGURES

LIST OF TABLES

Nomenclature

Description	**Symbols**
Elastic Modulus of specimen	E_s
Poisson's ratio of specimen	$Ʊ_s$
Reduced Modulus	E_r
Elastic Modulus of indenter	E_i
Poisson's ratio of indenter	$Ʊ_i$
Power law Constants	α
(From Curve fitting data)	m
Final Depth	h_f
Maximum Depth	h_{max}
Maximum Load	P_{max}
Sneddon's Correction factor	Ɛ
Slope	S
Contact Depth	h_c
Area Function	$A(h_c)$

1. INTRODUCTION

High performance fibers have strong anisotropy in their mechanical properties owing to the highly oriented chain molecules or crystals along the fiber axis. Measurement of mechanical properties at micro and nano scales could be very difficult especially for the single fibers having a diameter in range of 5 - 20 microns. There are many techniques available for the measurement of longitudinal modulus which is the modulus in the fiber axis direction whereas measurement of transverse modulus which is in normal direction to the fiber axis direction is very difficult because of the difficulty in the measurement change in fine diameter of these fibers. With the increasing applications high performance fibers, study of these properties at nano scales is very important. Very limited technology is available today for the quantitative measurement of mechanical properties at nano scale, one of which is Nano indentation. Various other methods are used to characterize the mechanical properties of fibers which include micro tension and micro bending. Bunsell [1] studied the tensile and fatigue behavior of Kevlar - 49. Ward et al [2, 3] measured the transverse modulus of polyethylene and some other thick polymeric micro filaments. The experimental method that was employed by ward et al. was that a monofilament was compressed between two parallel plates transversely to the fiber axis, and the amount of flattening of the contact area of the fiber resulting from the compression was measured with a microscope. The transverse modulus of the filament was then estimated from the size of the contact area and the compression force. These authors also showed that the transverse modulus could the estimated from the diametric change in the fiber caused by the transverse compression. In this project, a simulation of nanoindentation is carried out to find mechanical properties of the K-29 single fiber in the transverse direction of the fiber.

2. THEORY OF NANOINDENTATION

2.1. History

Nanoindentation is a technique used to find the mechanical properties of a material at nano and micro scale. The nanoindentation technique was developed in the mid-1970s to measure the hardness of small volumes of a material [4]. Over the past few decades, many researchers utilize this technique to measure the modulus, hardness, and the properties of thin films and coatings have used this technique.

Nanoindentation provides an insight to measure the mechanical properties of materials of very small volumes. A very sharp tip is used to measure the arbitrarily small volumes of a material, but this leads to difficulty in determining the indentation area. To address this issue various depth sensing indentation methods have been developed.

To measure the elastic modulus, the displacement of the indenter tip and the force during the indentation process is recorded and plotted in a graph. The slope of the unloading curve is used to calculate the elastic modulus. The most common unload curve analysis techniques are Oliver - Pharr [5] and Doerner-Nix [6] methods. According to the literature, either of these techniques is used to measure the elastic modulus of metals and the results are far from the actual tensile-test values. While the known elastic modulus of tungsten is 420 GPa, Doerner-Nix [6] found the value to be 480 GPa using the nanoindentation technique. Similarly, the known elastic modulus for aluminum is 70 GPa, but Rodriguez and Gutierrez found the elastic modulus of aluminum to be 80GPa [7]. Garrido Maneiro and Rodríguez [8] studied the nanoindentation with spherical–conical tips and observed an increasing elastic modulus with an increasing load for two aluminum alloys. This inflated elastic modulus value for metals is often attributed to the indentation pile-up, indent size effect, and the elastic recovery [9-12]. The indentation test is similar to the compression test [13-14] and the stress under an indenter is different than that in a round or flat bar in tension. Also, the lateral displacement of a material at the free surface around the edge of the indenter means that a uniaxial stress field is not maintained during unloading. On the other hand, nonmetallic materials, such as fused silica, soda-lime glass, and silicon, do not pile-up during indentation and therefore the unload curve provides good results of elastic modulus [5].

Figure 1 illustrates the load-displacement curve during nanoindentation where *P* represents load and *h* represents displacement of the indenter.

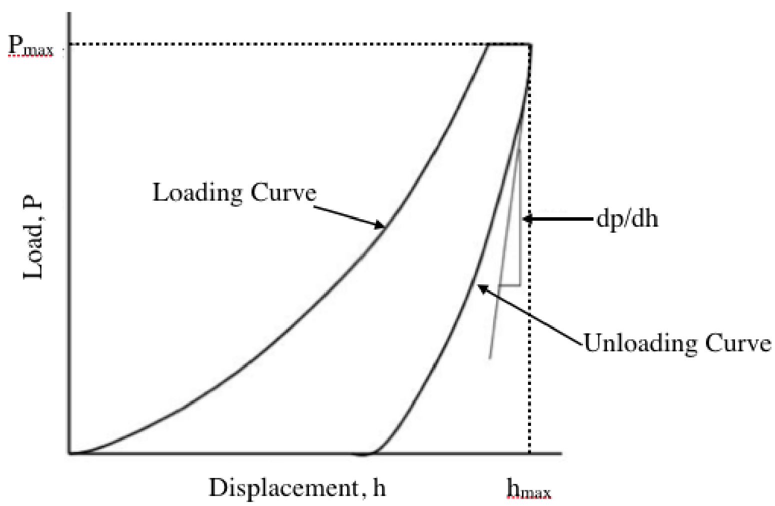

Figure 1: Schematic of load vs. displacement curve for an elastic-plastic material from a nano indenter with Berkovich indenter.

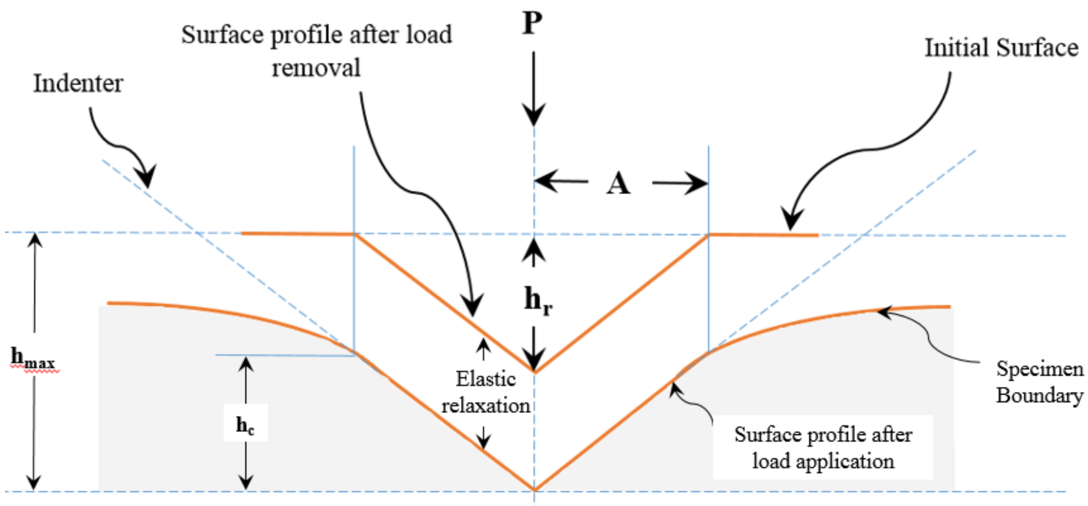

Figure 2: Schematics representation showing the quantities used in the analysis

P_{max} is the point at maximum applied load, slope of the unloading curve can be defined by slope $S = dp/dh$.

In the indentation process at the unloading stage the boundary of the test specimen make a rounded surface as shown in figure 2.

The elastic modulus is calculated using the following equation derived from the Hertzian theory of contact mechanics [24]:

$$\frac{1}{E_r} = \frac{(1 - \nu_s^2)}{E_s} + \frac{(1 - \nu_i^2)}{E_i} \tag{1}$$

The elastic modulus, E_s, the Poison ratio, ν_s, of the specimen, and the reduced modulus, E_r of the material can be calculated from Eqn (1).

The most accepted analysis method for calculating the slope of the indentation unload curve at maximum displacement is the Oliver-Pharr method [5]. In this method, the unload curve is described by the power-law:

$$P = \alpha(h_{max} - h_f)^m \tag{2}$$

The above equation is non-linear and numerical analysis techniques are used to determine the values of constants α and m. In this case, final depth, $h_f = 0$ as the indentation is elastic and there is no permanent mark on the specimen. All the data points of the curve are used for the fitting function. The slope S at the maximum displacement data point h_{max} can be calculated by taking the first derivative of Eqn (2).

$$S = \frac{dP}{dh} = \alpha m(h_{max} - h_f)^{(m-1)} \tag{3}$$

The indentation contact depth h_c is not equal to the total displacement h_{max} of the indenter into the sample because the surrounding surface has elastic relaxation during the process after the load is removed. According to Doerner-Nix [6] and Oliver-Pharr analysis methods [5], h_c can be calculated from Eqn (4) where Ɛ is a geometric correction factor to determine the edge effects at the contact perimeter.

$$h_c = h_{max} - \varepsilon(h_{max} - h_r) \tag{4}$$

$$h_r = h_{max} - \left(\frac{P_{max}}{S}\right) \tag{5}$$

By substituting the Eqn (5) in Eqn (4), the term h_r can be eliminated,

$$h_c = h_{max} - \varepsilon\left(h_{max} - \left[h_{max} - \left(\frac{P_{max}}{S}\right)\right]\right) \tag{6}$$

$$h_c = h_{max} - \varepsilon\left(\frac{P_{max}}{S}\right) \tag{7}$$

From Hertzian method theory [24]

$$E_r = \frac{1}{\beta}.\frac{\sqrt{\pi}}{2}.\frac{S}{\sqrt{A(h_c)}} \tag{8}$$

Where β is defined as the shape parameter for the indenter tip and it is generally assumed equal to 1 for Berkovich indenters [15-20].

Once h_c has been calculated, the area function is then approximated by a fitting polynomial [2-7] as in Eqn (9):

$$A(h_c) = C_0 h_c^2 + C_1 h_c + C_2 h_c^{1/2} + C_3 h_c^{1/4} + C_4 h_c^{1/8} + C_5 h_c^{1/16} + \cdots \tag{9}$$

Area function can be simple or complicated relationships. On a simpler side a function of the type $A(h_c) = C_0 h_c^2 + C_1 h_c$ is a reasonably robust approach which can be used for the modulus measurements to within about 2% of literature values across a width range of indentation depths. The higher order terms are used in the approximation of the indenter profile with a higher order polynomial fit to capture irregularity in the indenter surface which has an impact in the data at very small indentation depths. In this work, a 2nd order function is considered for the analysis as the indenter used in the experimental investigations is new and has minimum irregularities. Also, the indentation depth range used is this investigation is always more than 500nm.

2.2. Finite element analysis Theory

Abaqus is a general-purpose finite element code now maintained by Dassault Systemes. It uses large deformation nonlinear Lagrangian solid mechanics principles to model the response of a wide range of structures and systems to mechanical loading. The explicit methods calculate the state if the system at later time form the state of system at the current time, while implicit methods find a solution by solving an equation involving both current state and the later one. In this work, explicit analysis is used as implicit method is harder to implement as it is computationally heavy method. Also, a practically small time step was possible for the explicit method for the current simulation.

2.2.1. Explicit Dynamic Analysis

(a) Introduction

Explicit dynamic analysis uses finite strain theory and infinitesimal strain theory. It can be used to analyse:

- Relatively short dynamic response time of large models.
- Events and processes those are discontinuous.
- Contact definitions.
- Adiabatic stress when inelastic dissipation generates heat in a material.
- Quasi-static events for complex contact conditions.
- Automatic or fixed time incrimination to scale global time estimate.

The explicit dynamic method uses central-difference time integration rule and performs small time increments accurately in a large number. Each increment in this analysis is relatively inexpensive when compared to the increments in a direct-integration dynamic analysis. The dynamic equilibrium equations are satisfied at the beginning of the increment, t. The accelerations calculated at t, advance the velocity solution to time $t + \Delta t/2$ and the displacement solution to time$t + \Delta t$.

(b) Numerical Implementation

The explicit dynamic analysis method is based on explicit integration rule along with diagonal element mass matrices. The following equations for the motion of a body are combined with explicit central-difference integration rule:

$$\dot{u}^{N}_{\left(i+\frac{1}{2}\right)} = \dot{u}^{N}_{\left(i+\frac{1}{2}\right)} + \frac{\Delta t_{(i+1)} + \Delta t_{(i)}}{2}\ddot{u}^{N}_{(i)} \tag{10}$$

$$\dot{u}^{N}_{(i)} = \dot{u}^{N}_{(i)} + \Delta t_{(i+1)}\dot{u}^{N}_{(i+\frac{1}{2})} \tag{11}$$

Where, u^N = degree of freedom and i = number of increments, N represents the displacement or the rotational component

The central difference time integration method is explicit as the kinetic state is advanced using known values of $\dot{u}^{N}_{\left(i+\frac{1}{2}\right)}$ state at a later time step and $\ddot{u}^{N}_{(i)}$ state at the current time step of the previous increment.

The explicit method uses diagonal element mass matrices because lumped mass matrix inverse is easy to calculate.

The accelerations of the increment are calculated by:

$$\dot{u}^{N}_{(i)} = (M^{NJ})^{-1}(P^{J}_{(i)} - I^{J}_{(i)}) \quad (12)$$

Where, M^{NJ}= mass matrix, $P^{J}_{(i)}$= applied load vector, and $I^{J}_{(i)}$ = internal force vector.

The vector multiplication of the mass inverse by the inertial force requires *n* operations, with *n* denoting the number of degrees of freedom in a model. The explicit method does not require iterations and tangent stiffness matrix. The internal force vector, I^J is assembled from contributions from the individual elements such that a global stiffness matrix need not be formed.

(c) Nodal Mass and Inertia

Abaqus/Explicit requires a nonzero nodal mass or inertia at all translational degrees of freedom and nonzero rotary inertia at all rotational degrees of freedom unless any constraint are applied using the boundary conditions. More precisely, a nonzero nodal mass must exist unless all activated translational degrees of freedom are constrained and nonzero rotary inertia must exist unless all activated rotational degrees of freedom are constrained. Nodes of a rigid body and Eulerian elements do not require mass, but the whole rigid body should have mass and inertia unless any constraints are applied. When degrees of freedom at a node are activated by elements with a nonzero mass density like solid, shell, beam or mass and inertia elements, a nonzero nodal mass or inertia occurs naturally from the assemblage of lumped mass contributions.

(d) Stability

This explicit procedure integrates through time by using many small time increments. The central-difference operator is conditionally stable, and the stability limit for the operator (with no damping) is given in terms of the highest frequency of the system as

$$\Delta t \le \frac{2}{\omega_{max}} \tag{13}$$

While the stability time increment with damping is described as:

$$\Delta t \le \frac{2}{\omega_{max}}\left(\sqrt{1+\xi_{max}^2} - \xi_{max}\right) \tag{14}$$

Where ξ_{max} is the fraction of the critical damping, ω_{max}, with the highest frequency.

Damping reduces the stable time increment as rigid body motions are suppressed by the bulk viscosity. Therefore, in Abaqus/Explicit a small amount of damping is given in the form of bulk viscosity to control high frequency oscillations. Apart from bulk viscosity, physical damping such as dashpots or material damping can also be assigned.

(e) Estimating the Stable Time Increment Size

The stability limit is approximated to the smallest transit time of a dilatational wave across the elements in a mesh:

$$\Delta t \approx \frac{L_{min}}{c_d} \tag{15}$$

Where L_{min} = smallest element dimension in a mesh and c_d = dilatational wave speed in terms of λ_0 andμ_0, with λ_0 and μ_0 denoting effective Lame's constants

The element thickness, or cross-sectional dimensions, is not considered in determining the smallest element dimension for beams, conventional shells, and membranes. The stability limit is based on midplane, or membrane, dimensions, and depends on the transverse shear behaviour of the nodes when the transverse shear stiffness is defined for shell elements. This value of ΔT is not a conservative approximation because damping, bulk viscosity and penalty contact stiffness are not considered at this stage. Therefore, the actual stable time increment chosen by Abaqus/Explicit is always less than the estimate by a factor between $1/\sqrt{2}$ and 1 in a two-dimensional model and between $1/\sqrt{3}$ and 1 in a three-dimensional model. The stable time increment is also dependent on the stiffness behaviour of a model with a penalty contact which is helpful in the reduction of the computational cost.

(f) Stable Time Increment Report

During the data check phase of analysis, Abaqus/Explicit writes a report to the status (.sta) file. The report contains an estimate of the minimum stable time and the smallest stable time increments of the elements. Initially, the stable time increments do not include damping, mass scaling, or penalty contact effects. As the simulation progresses then this parameter are accounted for in the calculation of the stable time step.

Few elements have smaller stability limits. The stable limit can be increased by increasing the size of the controlling element or by using mass scaling, therefore modifying the mesh. In this work we used an optimised mesh size for the computational cost and stable time step without using any mass scaling factor.

(g) Dilatational Wave Speed

In Abaqus/Explicit, the current dilatational wave speed, c_d is determined by calculating the effective hypo elastic material moduli from the material's constitutive response. By employing the effective Lamé's constants $\hat{\lambda}$ and $\hat{G} = 2\hat{\mu}$ one may utilize a hypo elastic stress-strain rule of the form of:

$$\Delta P = (3\hat{\lambda} + 2\hat{\mu})\Delta\epsilon_{vol} \tag{16}$$

With ΔPdefined as the increment in the mean stress, ΔS the increment in the deviatroic stress, $\Delta\epsilon_{vol}$ the increment of volumetric strain, and Δe the deviatroic strain increment. The effective Lamé's constant, $\hat{\lambda}$, in an isotropic elastic material is defined in terms of Young's modulus, E, and Poisson's ratio, ν as

$$\hat{\lambda} = \lambda_0 = \frac{E\nu}{(1+\nu)(1-2\nu)} \tag{17}$$

And

$$\hat{\mu} = \mu_0 = \frac{E}{2(1+\nu)} \tag{18}$$

The effective moduli, $\widehat{K}$, $\hat{\mu}$, are then calculated as:

$$3\widehat{K} = \left(3\hat{\lambda} + 2\hat{\mu}\right) = \frac{\Delta P}{\Delta\epsilon_{vol}} \tag{19}$$

with

$$(2\hat{\mu}) = \frac{\Delta S :\ \Delta e}{\Delta e :\ \Delta e} \tag{20}$$

The effective moduli, $\widehat{K}, \hat{\mu}$ for the shell elements that require numerical integration is calculated by integrating the effective moduli at the section points through thickness. Effective moduli represent the element stiffness and calculate the current dilatational wave speed in the elements as follows:

$$c_d = \sqrt{\frac{\hat{\lambda} + 2\hat{\mu}}{\rho}} \tag{21}$$

(h) Time Increment

In explicit dynamic analysis, the time increment must be smaller than the stability limit of the central-difference operator. Large time increment results in an unstable solution. Therefore, the response of solution variables such as displacement oscillates with increasing amplitudes. The total energy balance also changes.

The initial increment is directly proportional to the size of the smallest element in the mesh if the model is of single material type. The element with the highest wave speed determines the initial time increment if the mesh contains uniform size elements with multiple material descriptions.

(i) Scaling the Time Increment

To decrease the instability of a solution, adjust the stable time increment calculated by Abaqus/Explicit by a constant scaling factor.

Constant scaling factor can be used to scale the default global time estimates, the element-by-element estimates, or the initial element-by-element estimate.

(j) Automatic Time Increment

In Abaqus/Explicit, the default time increment is completely automatic. The stability limit is determined by element-by-element and global estimates. Element-by-element method is used to begin the analysis and the global estimation method is used later, if required.

(k) Element-by-Element Estimation

Initially, Abaqus/Explicit uses stability limit depending on the highest element frequency. The element-by-element estimate is calculated using the current dilatational wave speed in each element.

This estimation gives a smaller stable time increment than the true stability, which is dependent on the maximum frequency of the model. Boundary conditions and kinematic contact have the effect of suppressing the Eigen vale spectrum. Now, the global stability estimates can be used to make the time increment less sensitive to element size.

(l) Global Estimation

Global estimator determines the stability limit unless the fixed time increment is specified. After the algorithm determines the accuracy of the global estimation method, the switch to the global estimation method takes place.

The global estimation algorithm uses the speed of the current dilatational wave to determine the maximum frequency of the model. The global estimator allows time increments that exceed the element-by-element values.

(m) Fixed Time Increment

Initial element-by-element stability estimate or a user-specified time increment determines a fixed time Increment. Fixed time increment is useful for accurate representation of higher mode response of a problem. The dilatational wave speed in each element is used to compute the fixed time increment size.

3. METHODS

3.1. Experimental Setup

The sample that is used for the measurement is KM2 Kevlar. The diameter of a single fiber is estimated to be 12µm. In this study to measure the transverse elastic modulus of a single fiber, the sample is prepared by picking a single fiber from a yarn with a length of 8 inches. To isolate a single fiber from the yarn it is placed on a black background for a better visibility. An SEM puck is used as a mount for the fiber to be placed in the instrumented indentation machine. The fiber is attached with two washers using Cyanoacrylate (CA) glue as shown in the Figure 3a. The glue is then used for binding the fiber to the mount. The glue is applied on either ends of the mount as shown in Figure 3b. The adhesive is left undisturbed to cure overnight for binding. During this process, a minimal amount of prestretch is applied to the fiber which is then relaxed during the curing process of the glue.

Instrumented indentation tests are performed using a NanoTest Vantage manufactured by Micro Materials with a diamond indenter with Berkovich tip. Indentations should be performed at least 100µm away from the glued area. Load-controlled indentations are performed at various loads ranging from 1mN to 40mN, and then the indentations are performed on the fiber using NanoTest Vantage using Continuous stiffness measurement (CSM) method. In the instrumented indentation process the total compliance is the sum on machine compliance structural compliance [21-26]. The machine compliance is estimated by calibrating the machine with known materials.

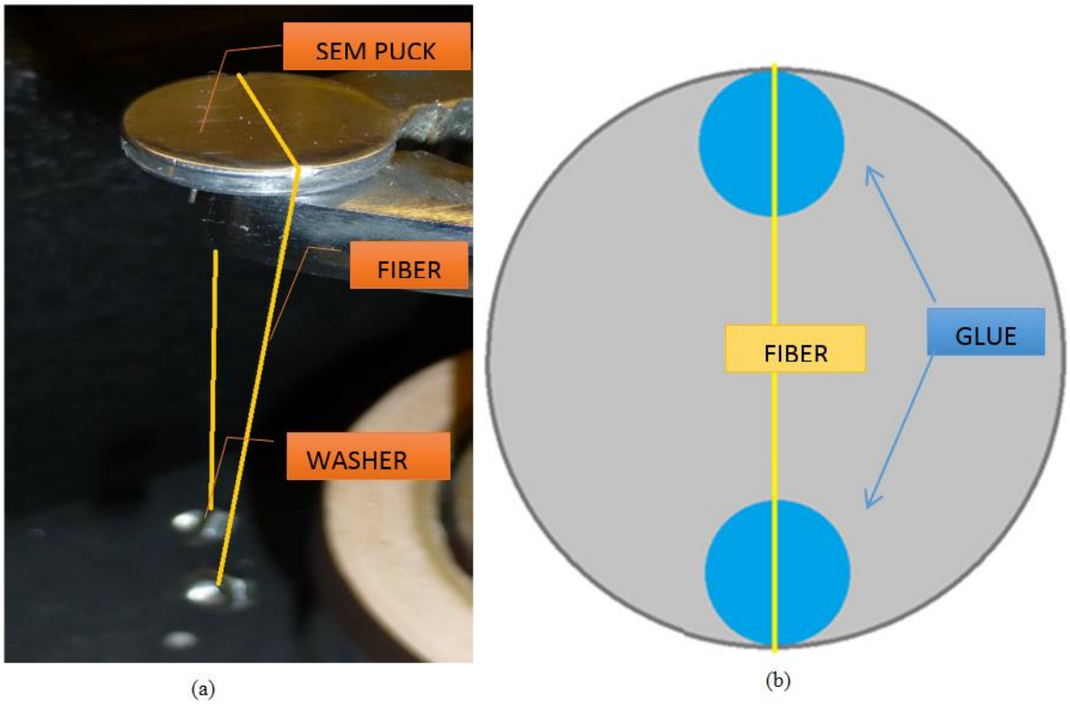

Figure 3: (a) Kevlar single fiber is mounted on polished SEM puck, pretension measured by hanging two 1.1g washers (b) Placement of the glue to constrain the fiber movement over the SEM puck for indentation

3.2. Simulation method

Load-displacement curves are the results from the indentation test. As explained in the previous section, the unloading curve is used for determining hardness and reduced modulus, and this calculation requires the area function, or projected indentation area at a given depth. However, this assumes that the triangular indent is being placed on a flat surface. The indentations on the KM2 specimens are performed on a cylindrical surface, which requires modified equations to determine the area function and subsequently, the hardness and reduced modulus. The novel idea behind this research is to use a combination of simulations and experimental data to produce a way to calculate these values for nanometer-diameter fibers using indentation.

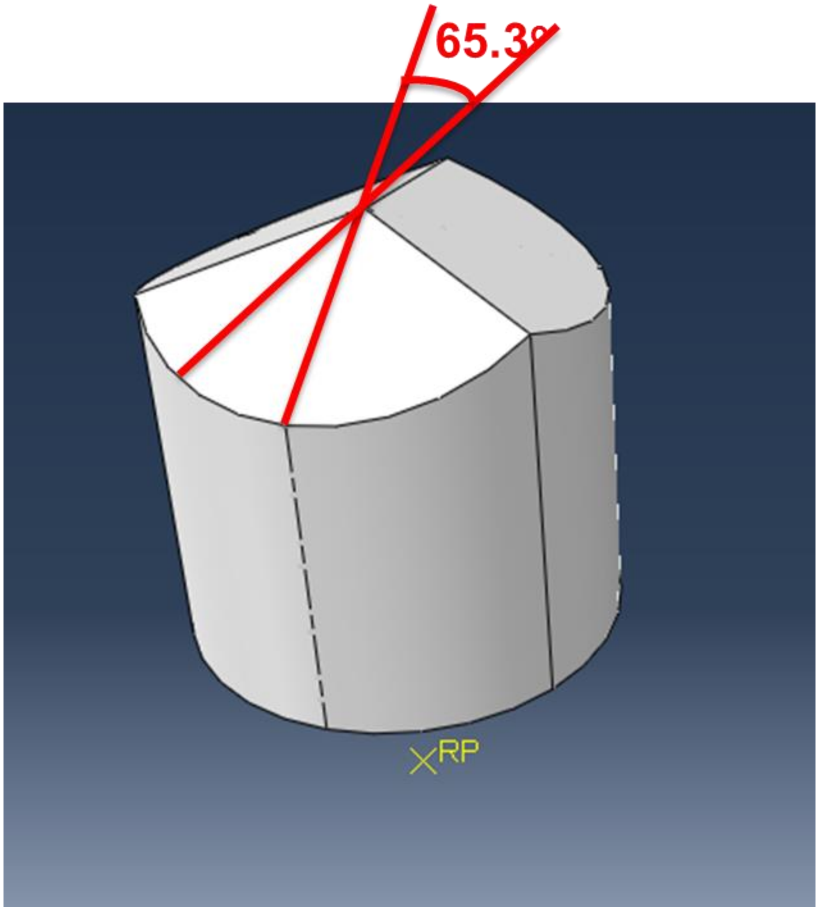

Figure 4: Schematic illustration of Berkovich Indenter

In this work, a commercial FEA software ABAQUS is used for the simulation of elastic behavior of the material in the nanoindentation process. A 3D model was employed to represent a Berkovich indenter tip. The Berkovich geometry consists of a 3-sided pyramid with a half angle of 65.3^{o}. A 100 nm tip curvature is modeled to symbolize the indenter used in the experiment as shown in the Figure 4. The KM2 specimen is modeled as a cylinder representing fiber section with 100 µm length and variable diameter as shown in Figure 6.

The specimen and the indenter are meshed with C3D8R, which is continuum three dimensional eight node quadrilateral, reduced integration elements. In the indentation process, deformation is mainly concentrated at the point of contact of the indenter and the specimen; a denser mesh is used at the indentation area of the specimen to capture the stress distribution. In order to reduce the computational time a coarser mesh was used in the areas away from the indenter contact point on the specimen. Various specimens with diameter ranging from 7 µm to 50 µm are used to simulate the indentation process.

The fiber material is considered to be elastic and homogenous isotropic with young's modulus, E = 70 GPa as this is the material property of quartz. Quartz is used for the area function calibration in instrumented indentation as the properties are well known. . This approximation is strictly used for the calculation of geometry of the contact surface between the indenter and specimen. Each specimen is then simulated using three different values of Poisson's ratio $\nu_s = 0.15, 0.21, 0.33$ in order to check the sensitivity of the results over change in the Poisson's ratio. The elements of the indenter were defined as rigid element, which does not undergo any deformation. This approximation is used for the computational analysis as it reduced one term from the equation (1). All these are considered to be quasi static with no internal deformations or rigid body motion.

The contact boundary condition between the indenter tip and the specimen is defined as frictionless surface-to-surface contact in which the indenter surface is the master surface and the surface of the specimen is the slave. The contact direction was defined from indenter surface to the specimen so that the master surface penetrates into the slave allowing deformation of the sample upon contact. The boundary condition for the specimen was modeled as a fixed support at the lower edge to prevent movement and rolling.

As an elastic material model is defined for the specimen, the simulation process of the indentation is defined by single step loading with displacement of indenter into the specimen as boundary condition. A mesh convergence analysis is done to eliminate the mesh dependence on the results as shown in the Figure 5.

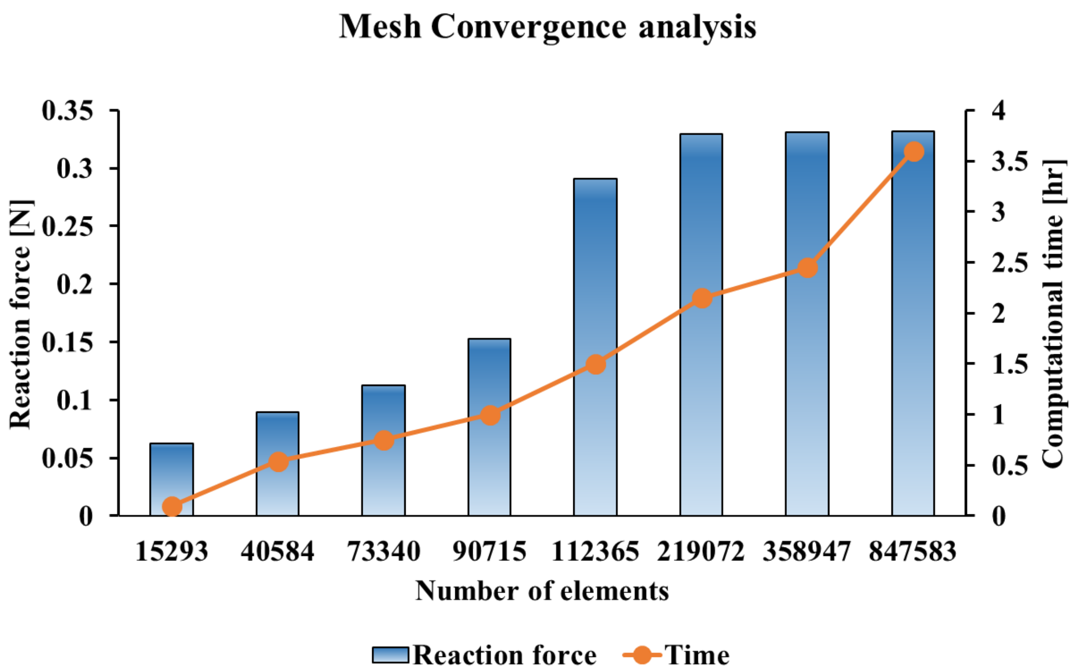

Figure 5: Mesh convergence analysis

To validate the model another specimen with flat surface is created and meshed using the same elements and boundary conditions described above and the model used as shown in Figure 7. The material properties of quartz were used to compare the results with the experiments. The area function is calculated for the obtained load – displacement graph from the simulation of the flat specimen. The calculated function is $A(h_c) = 22.25h_c^2 + 2914h_c$ which is very near to the area function calibrated in the experimental analysis.

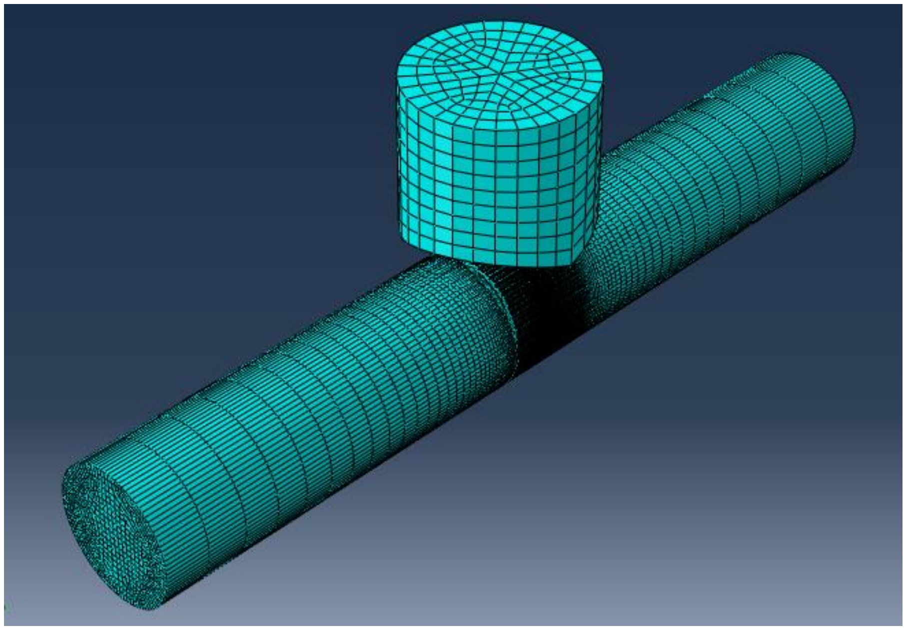

Figure 6: Finite element mode of indenter and specimen

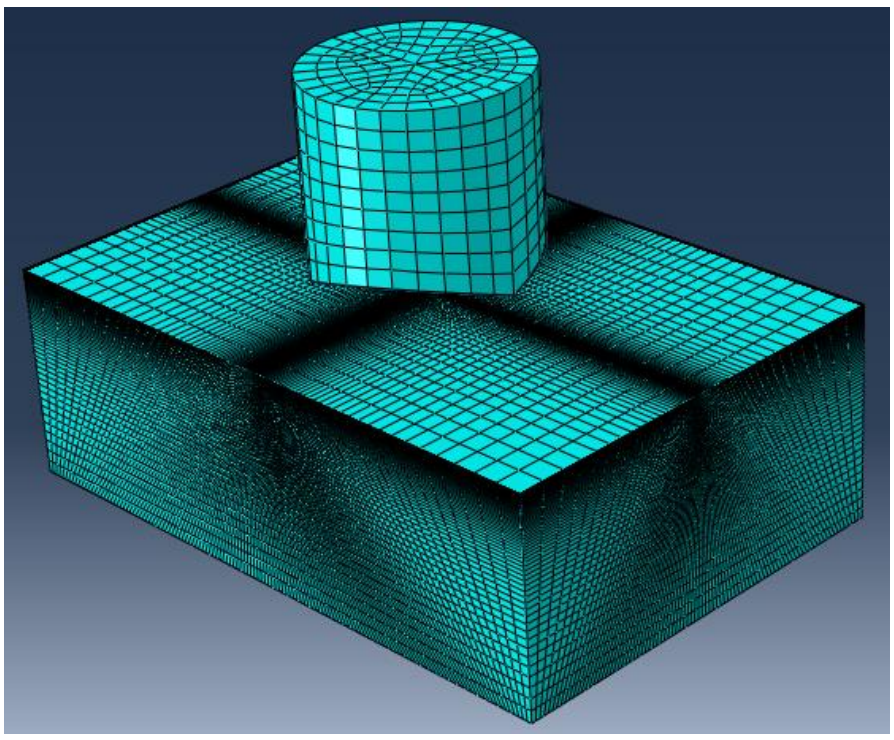

Figure 7: Finite element model for validation with flat specimen

4. RESULTS AND DISCUSSION

4.1. Simulation Results

Analysis was performed on different diameter fibers with 7, 15, 30, 40 and 50 µm diameter fibers with Berkovich indenter with indentation depths up to 2µm. As the material model used for the specimen is isotropic and only elastic properties are considered. The reaction force vs. indenter displacement for the various fibers is shown in the Plot 1 and Plot 2 at different indentation depths.

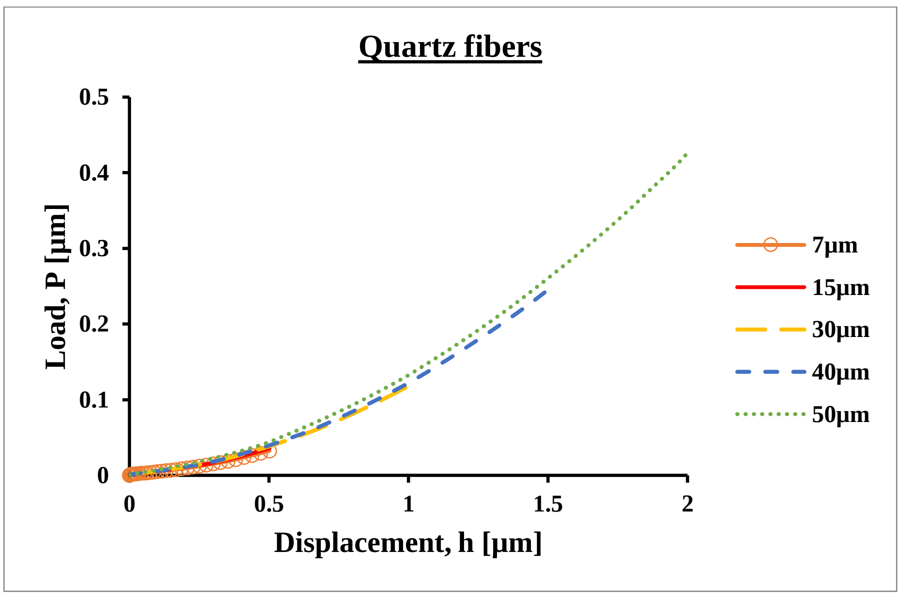

Figure 8: Load Vs Displacement of various diameter fibers with an indentation depth of up to 2 microns. Various displacements are considered according to the diameter of the fiber so that the shape of the fiber does not disintegrate at final indentation depth

Indentation depths at each diameter of a fiber are chosen carefully such that there is no shape deformation at the depths. At each diameter, analysis is performed at two depths, which are tabulated in Table 1.

Table 1: Indentation depth for various fiber diameters used in the simulation to calculate the load

Diameter [µm]	**Depth 1 [nm]**	**Depth 2 [nm]**
7	500	350
15	500	350
30	1000	500
40	1500	1000
50	2000	1000

4.2. Area function calculation by Simulation method

A straightforward approach for the measurement of the elastic modulus from nanoindentation is explained in the above section. But, to find the area function a bottom up approach is used. Figure 9 explains the schematics of area function calculation. A known material property is assigned to the model and the indentation process is simulated to reach a prescribed displacement. The reaction force experienced by the tip of the indenter is taken as output from the simulation. The results are as shown in Figure 8. As the material properties for the model are known the area function can be calculated for these values to fit the equation.

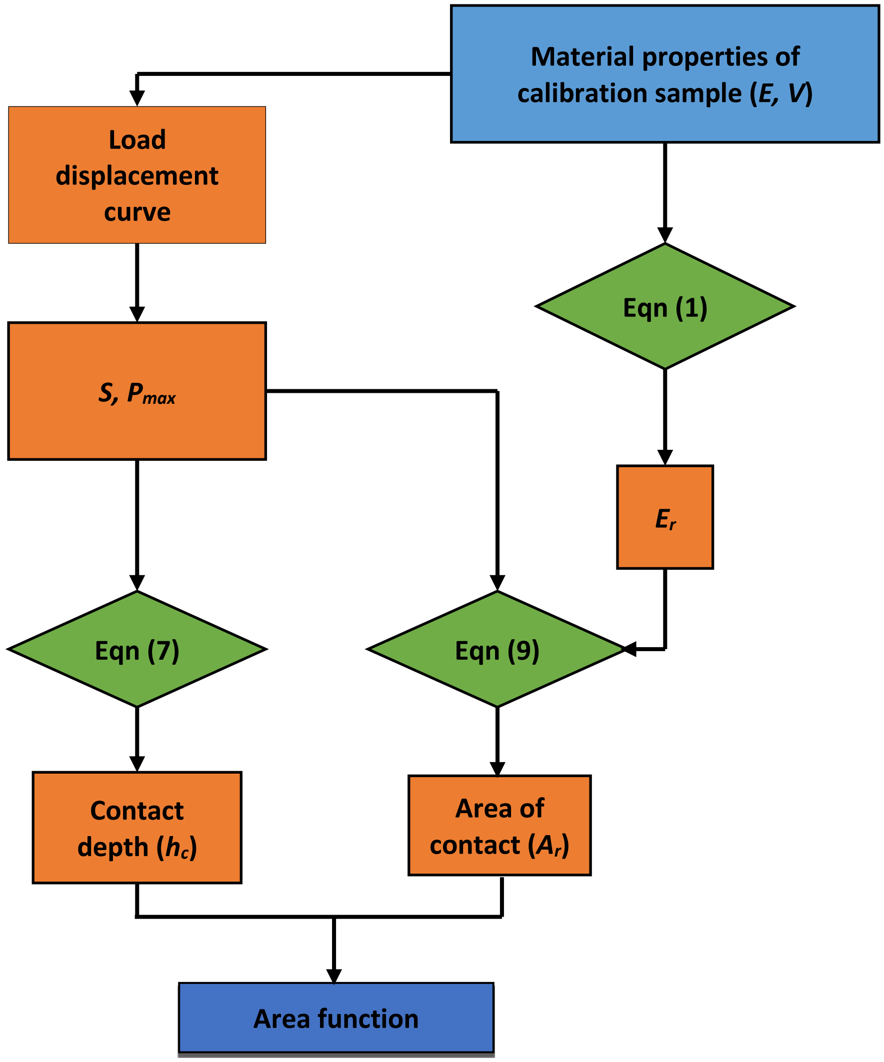

Figure 9: Schematic for the calculation of area function of the sample with circular geometry where material properties of the sample are known

A finite element model was developed using Abaqus to determine the area function for the indentation of cylindrical specimens. With the use of the solver in the software package various types of specimens with different parameters to obtain the load - displacement data for the indentation.

Area function is considered to a second-degree polynomial. Eliminating all the higher order terms from the Eqn (9), the area function equation takes the following form:

$$A(h_c) = C_0 h_c^2 + C_1 h_c \tag{22}$$

Analysis was first performed on a flat specimen and fibers with 7, 15, 30, 40, 50 µm diameters with Berkovich indenter with indentation depths up to 2µm.

Material Properties:

Elastic modulus: 70 GPa
Poisson's ratio: 0.21
Fiber diameter: 7 microns
Material Model: Linear elastic

(a) Case –I: Indentation depth 2µm i.e. h_{max} = 500nm and Ɛ = 0.75

E_r can be computed from Eqn (1)

$$E_r = 0.066913\ N/\mu m^2 \tag{23}$$

Stiffness can be calculated by Eqn (2), where Values of α and m are computed from power law fit analytically using least square method considering all data point in the curve.

$$\alpha = 0.0960 \text{ And m} = 1.6065 \tag{24}$$

Here as the material model is isotropic and homogenous, indentation does not leave any mark after the process and the final depth of zero i.e. h_f = 0

From Eqn (2),

$$S = 0.083 \tag{25}$$

Eqn (7) can find contact depth

$$h_c = 0.20748\ \mu m \tag{26}$$

Area of the indent can be found for the known material by using Eqn (9)

$$A(h_c) = 1.2011196\ \mu m^2 \tag{27}$$

Equation the known area to the area function with calculated contact depth, we get

$$A(h_c) = 0.043\ C_0 + 0.2075\ C_1 \tag{28}$$

(b) Case – II: Indentation depth 1 µm i.e. h_{max} = 350 nm and Ɛ = 0.75

E_r can be computed from Eqn (1)

$$E_r = 0.066913\ N/\mu m^2 \tag{29}$$

Stiffness can be calculated by Eqn (2), where

Values of α and m can be computed from power law fit analytically using least square method.

$$\alpha = 0.0960 \text{ And m} = 1.6065 \tag{30}$$

Here as the material model is isotropic and homogenous, indentation does not leave any mark after the process and the final depth of zero i.e. $h_f = 0$

From Eqn (2),

$$S = 0.060 \tag{31}$$

Contact depth can be found by Eqn (7)

$$h_c = 0.11730\ \mu m \tag{32}$$

Area of the indent can be found for the known material by using Eqn (9)

$$A(h_c) = 0.6275\ \mu m^2 \tag{33}$$

Equation the known area to the area function with calculated contact depth, we get

$$A(h_c) = 0.0138 C_0 + 0.1173\ C_1 \tag{34}$$

Therefore, the calculated area function is

$$A(h_c) = 3.89945\ h_c^2 + 4.77312\ h_c \tag{35}$$

4.3. Observations

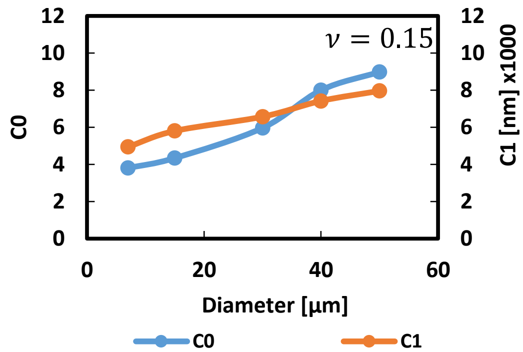

(a)

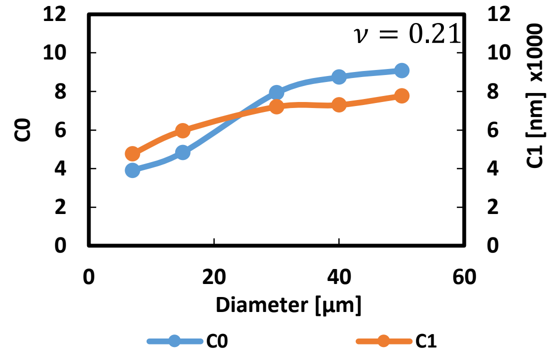

(b)

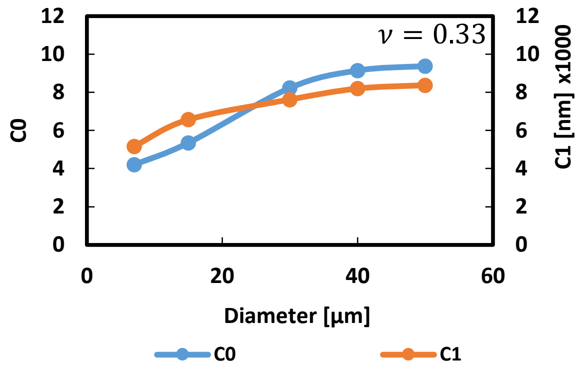

(c)

Figure 10: C_0 and C_1 at various diameter of the fiber samples Poisson's ratio at (a) 0.15, (b) 0.21, and (c) 0.33

The derived equations for the constants with respect to the diameter of a fiber include the correction for the rounded surface from the assumption of semi-infinite plane that are averaged over various Poisson's ratios:

$$C_0 = 2.791 \ln(D) - 1.9447 \tag{36}$$

$$C_1 = 1.547 \ln(D) + 1.9323 \quad (37)$$

The above equations are in 95% agreement with the actual scenario. The extrapolated value of the C0 equation at very large diameters is around 25 which are in complete agreement with the literature C0 value for Berkovich indenter, which are around 24.5.

Therefore, the elastic modulus found using the area function calculated from the equations (11) and (12) is true to 95% confidence.

The general equation for the area function derived from the analysis is

$$A_r(h_c) = [2.791 \ln(D) - 1.9447]h_c^2 + [1.547 \ln(D) + 1.9323]h_c \quad (38)$$

4.4. Experimental results

KM2 fiber is used as a test specimen for the experiments to determine the transverse mechanical properties of the fiber using the method discussed in section 4.2. Figure 8 explains the typical load-displacement curves from the instrumented indentation at various loads ranging from 5mN to 40mN. The mechanical properties determined through the traditional indentation theory assume the sample to have a semi-infinite plane. In the present study, the sample has a curvature. This curvature can be accounted by using the method explained in the section 4.2 to find the projected contact area to obtain the material properties.

The indentations are performed with maximum load as boundary condition, starting from a load of 5mN where the displacement of the indenter is around 1200nm. The fiber has a coating of 200nm. As the load is increased displacement of the indenter increases. 10

indents are performed at each load as light deviation can be accounted for the surface roughness, which may be local morphological defect on the fiber surface. Also, deviation in the indentation data is more after the depth of 2000nm as at this point the coating is completely pierced and the indenter touches the fibrils. This can be seen in Figures 9d, 9e and 9f.

In Figure 11 the experimental load vs. indentation data at different loads is plotted. The bend in the indentation data in the unloading curve is due to thermal drift. This parameter is taken into account in the post processing in the calculation of indentation modulus.

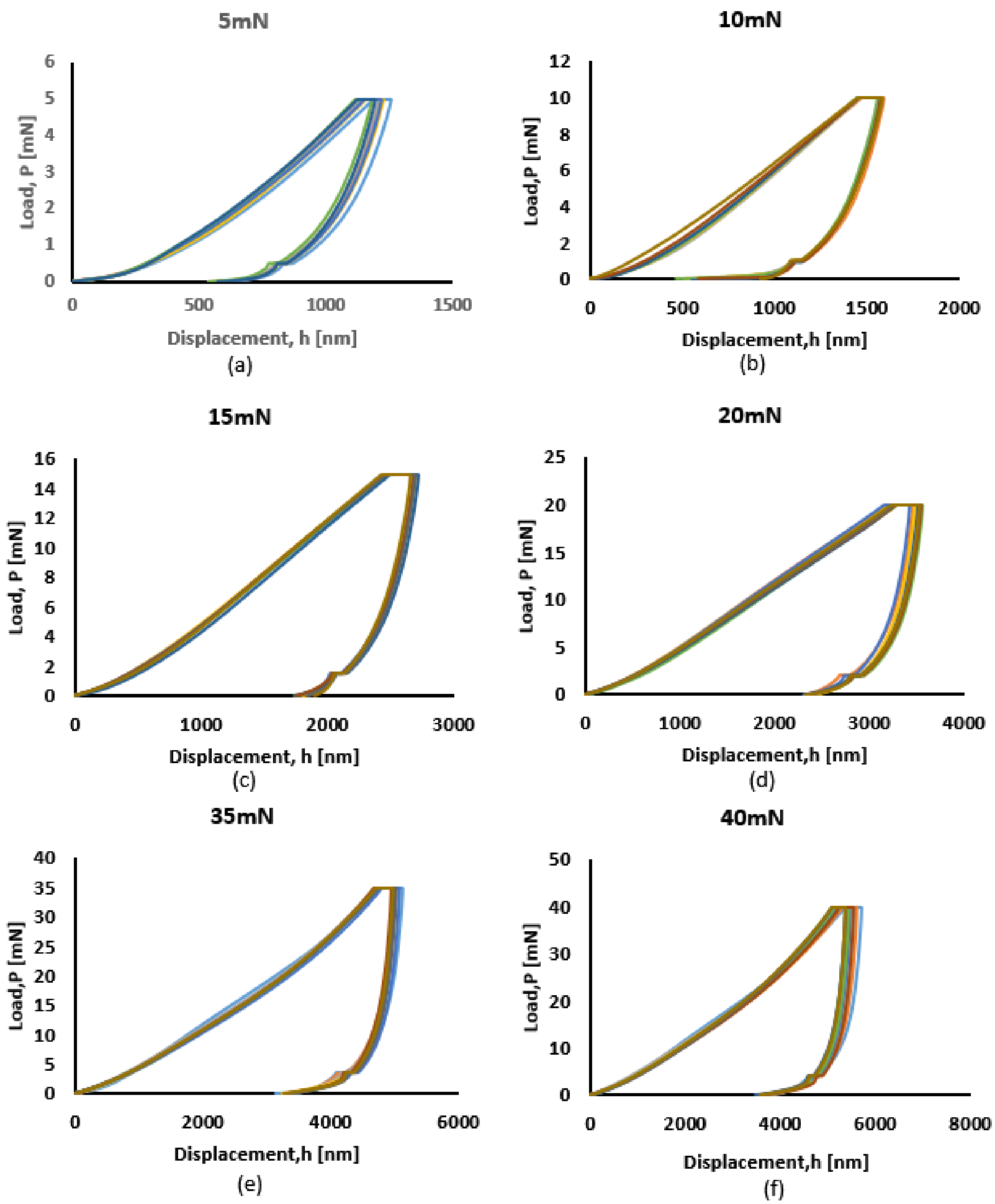

Figure 11: Load Vs displacement data obtained from the Berkovich indenter on KM2 fiber at different load (a) 5mN (b) 10mN (c) 15mN (d) 20mN (e) 35mN (d) 40mN. At each load, at least 7 indents were performed to ensure repeatability.

The load vs. displacement data obtained from the instrumented indentation process is used in the calculation of elastic modulus of a fiber in the transverse direction as described in Figure 10.

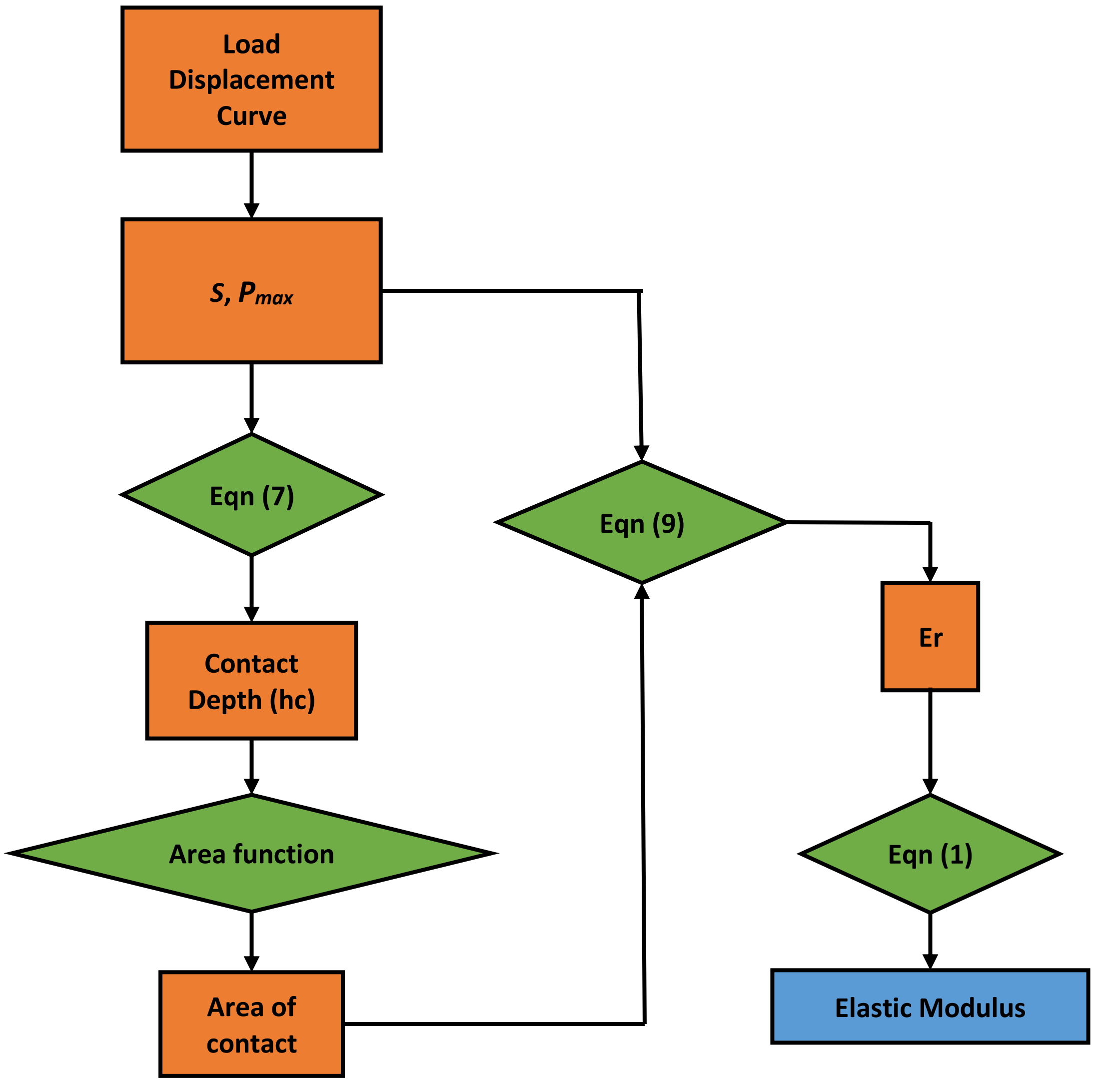

Figure 12: Flow charts showing the calculation of elastic modulus from instrumented indentation process

Elastic modulus of the KM2 fiber is calculated from Eqn (1) – Eqn (9) as shown in the above Figure 12 with the experimental data. Area function correction for the circular geometry compliance is calculated from the function derived by the simulation method. The material properties of the diamond indenter used in the experiment are E = 1,250 GPa and ν = 0.33. The only value assumed here is the Poisson's ratio of the sample which is $\nu_s = 0.27$ [27]. The transverse modulus of the KM2 fiber is estimated to be $7.76 \pm 0.22\ GPa$.

In reality these fibers are viscoelastic and they undergo plastic deformations during the indentation process. For the calculation of the elastic modulus only the linear region of the unloading curve is taken into consideration. This corresponds to around 40% of the curve data from the start of unloading curve. The final contact depth also depends on plastic properties of the fiber as well. But plasticity is a diversely nonlinear phenomenon and it is very difficult to quantitatively generalize plastic behavior of the different materials to one constitutive model.

The approximation in the simulation for an elastic model has a good fit to the experimental data as the linear region of the unloading curve in the test data captures the elastic properties of the material. Therefore, this is considered to be a valid approximation for the quantifying the geometric compliance of the fiber with respect to is physical shape.

For comparison, the transverse elastic modulus of the fibers found through general Oliver and Pharr [5] analysis is 3.5 ± 0.83 GPa. The results agree reasonably well with the previously reported values of transverse elastic modulus for KM2 fiber. The reported values are 7.74 ± 0.96 GPa [27] and 6.2 ± 1.00 GPa [20]. In these reported values from McAllister et al [19-20] the area function correction is geometrically calculated with the approximation of projected surface area of the conical indenter is equivalent to that of Berkovich indenter. The Berkovich indenter has three edges which is in contact with the material with a greater stiffness than the other surfaces because of which prediction of elastic modulus is higher in case of Berkovich indenter in comparison with the conical indenter where all of the indenter surface is equally in contact with the sample.

In this study, as the indenter model used is identical to Berkovich the results of elastic modulus are as predicted and are on the higher side than the estimation of correction with the conical geometry approximation for Berkovich. Also, it can be seen that the function had relatively less error and also the area function is a parametric function of diameter of the fiber which means, using this function, projected area of the Berkovich indenter can be accurately calculated for various diameters of fibers.

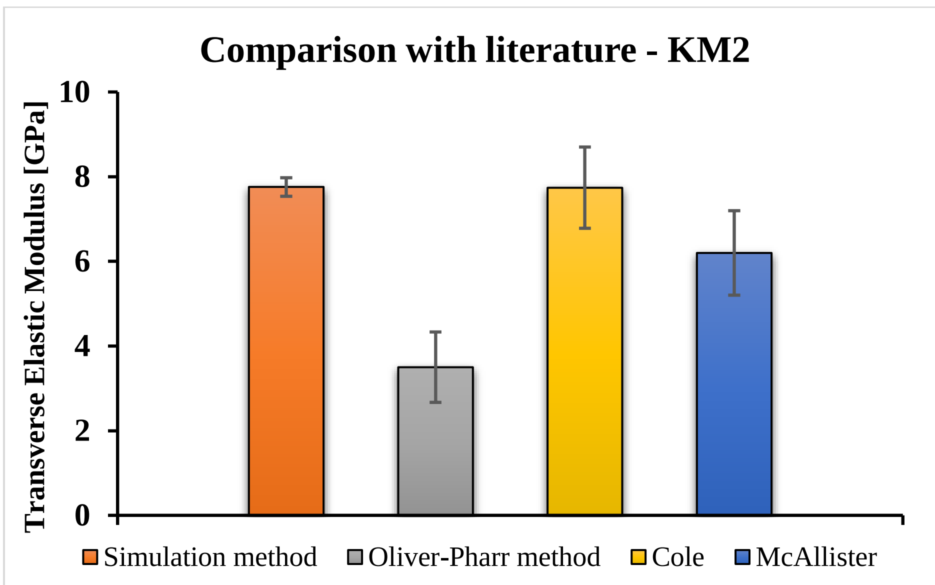

Figure 13: Comparison of elastic modulus values for KM2

5. CONCLUSIONS

In this study, nanoindentation techniques are used to estimate the elastic modulus of circular of the fibers and this calculation requires the area function, or projected indentation area at a given depth. As indentation theory assumes that the triangular indent is being placed on a semi-infinite flat surface, general area function cannot predict accurate projected area on a circular specimen. The indentations on cylindrical surface require modified equations to determine the area function and subsequently, the hardness and reduced modulus. Therefore, a combination of simulations and experimental data is used to produce an area function $A(h_c) = [2.791\ln(D) - 1.9447]h_c^2 + \left[1.547\ln(D) + 1.9323\right]h_c$ which includes the corrections for the convex geometry of the fiber surface.

This calculation method is then validated with experimental studies using instrumented indentation of KM2 fibers. The calculated elastic modulus for KM2 was estimated to be 7.76±0.22 GPa which compares favorably with values found in literature.

REFERENCES

[1] Bunsell, A.D., 1975. The tensile and fatigue behaviour of Kevlar-49 (PRD-49) fibre. *Journal of Materials Science*, *10*(8), pp.1300-1308.

[2] Hadley, D.W., Ward, I.M. and Ward, J., 1965, April. The transverse compression of anisotropic fiber monofilaments. In *Proceedings of the Royal Society of London A: Mathematical, Physical and Engineering Sciences* (Vol. 285, No. 1401, pp. 275-286). The Royal Society.

[3] Pinnock, P.R., Ward, I.M. and Wolfe, J.M., 1966, April. The compression of anisotropic fiber monofilaments. II. In *Proceedings of the Royal Society of London A: Mathematical, Physical and Engineering Sciences* (Vol. 291, No. 1425, pp. 267-278). The Royal Society.

[4] Poon, B., Rittel, D. and Ravichandran, G., 2008. An analysis of nanoindentation in linearly elastic solids. *International Journal of Solids and Structures*, *45*(24), pp.6018-6033.

[5] Oliver, W.C. and Pharr, G.M., 1992. An improved technique for determining hardness and elastic modulus using load and displacement sensing indentation experiments. *Journal of materials research*, *7*(6), pp.1564-1583.

[6] Doerner, M.F. and Nix, W.D., 1986. A method for interpreting the data from depth-sensing indentation instruments. *Journal of Materials research*, *1*(4), pp.601-609.

[7] Maneiro, M.G. and Rodríguez, J., 2005. Pile-up effect on nanoindentation tests with spherical–conical tips. *Scripta materialia*, *52*(7), pp.593-598.

[8] Sargent, P.M. and Page, T.F., 1981. The possible effect of elastic recovery on the microhardness of anisotropic materials. *Scripta Metallurgica*, *15*(3), pp.245-250.

[9] Kalman, D.P., Merrill, R.L., Wagner, N.J. and Wetzel, E.D., 2009. Effect of particle hardness on the penetration behavior of fabrics intercalated with dry particles and concentrated particle− fluid suspensions. *ACS applied materials & interfaces*, *1*(11), pp.2602-2612.

[10] Decker, M.J., Egres, R.G., Wetzel, E.D. and Wagner, N.J., 2005, November. Low velocity ballistic properties of shear thickening fluid (STF)–fabric composites. In *Proceedings of 22nd International Symposium on Ballistics, in Vancouver, BC, Canada* (pp. 18-25). Lancaster, PA: DESTech Publications.

[11] Riekel, C. and Davies, R.J., 2005. Applications of synchrotron radiation micro-focus techniques to the study of polymer and biopolymer fibers. *Current opinion in colloid & interface science*, *9*(6), pp.396-403.

[12] Li, S.F.Y., McGhie, A.J. and Tang, S.L., 1994. Comparative study of the internal structures of Kevlar and spider silk by atomic force microscopy. *Journal of Vacuum Science & Technology A: Vacuum, Surfaces, and Films*, *12*(4), pp.1891-1894.

[13] Cheng, M., Chen, W. and Weerasooriya, T., 2005. Mechanical properties of Kevlar® KM2 single fiber. *Journal of Engineering Materials and Technology*, *127*(2), pp.197-203.

[14] Deteresa, S.J., Allen, S.R., Farris, R.J. and Porter, R.S., 1984. Compressive and torsional behaviour of Kevlar 49 fiber. *Journal of Materials Science*, *19*(1), pp.57-72.

[15] Kawabata, S., 1990. Measurement of the transverse mechanical properties of high-performance fibers. *Journal of the Textile Institute*, *81*(4), pp.432-447.

[16] Leal, A.A., Deitzel, J.M. and Gillespie Jr, J.W., 2009. Compressive strength analysis for high performance fibers with different modulus in tension and compression. *Journal of composite materials*, *43*(6), pp.661-674.

[17] Singletary, J., Davis, H., Ramasubramanian, M.K., Knoff, W. and Toney, M., 2000. The transverse compression of PPTA fibers Part I Single fiber transverse compression testing. *Journal of Materials Science*, *35*(3), pp.573-581.

[18] Singletary, J., Davis, H., Song, Y., Ramasubramanian, M.K. and Knoff, W., 2000. The transverse compression of PPTA fibers Part II Fiber transverse structure. *Journal of materials science*, *35*(3), pp.583-592.

[19] McAllister, Q.P., Gillespie, J.W. and VanLandingham, M.R., 2012. Evaluation of the three-dimensional properties of Kevlar across length scales. *Journal of Materials Research*, *27*(14), pp.1824-1837.

[20] McAllister, Q.P., Gillespie, J.W. and VanLandingham, M.R., 2012. Nonlinear indentation of fibers. *Journal of Materials Research*, *27*(1), pp.197-213.

[21] Jakes, J.E., Frihart, C.R., Beecher, J.F., Moon, R.J. and Stone, D.S., 2008. Experimental method to account for structural compliance in nanoindentation measurements. *Journal of Materials Research*, *23*(4), pp.1113-1127.

[22] Gindl, W. and Schöberl, T., 2004. The significance of the elastic modulus of wood cell walls obtained from nanoindentation measurements. *Composites Part A: Applied Science and Manufacturing*, *35*(11), pp.1345-1349.

[23] Hanson, M.T., 1992. The elastic field for conical indentation including sliding friction for transverse isotropy. *J. appl. Mech*, *59*(2), pp.S123-S130.

[24] Hanson, M.T., 1992. The elastic field for spherical Hertzian contact including sliding friction for transverse isotropy. *a a*, *2*, p.a2.

[25] Vlassak, J.J. and Nix, W.D., 1994. Measuring the elastic properties of anisotropic materials by means of indentation experiments. *Journal of the Mechanics and Physics of Solids*, *42*(8), pp.1223-1245.

[26] Swadener, J.G. and Pharr, G.M., 2001. Indentation of elastically anisotropic half-spaces by cones and parabolae of revolution. *Philosophical Magazine A*, *81*(2), pp.447-466.

[27] Cole, D.P. and Strawhecker, K.E., 2014. An improved instrumented indentation technique for single microfibers. *Journal of Materials Research*, *29*(9), pp.1104-1112.